Atmospheric Research 342 (2026) 109135

Contents lists available at ScienceDirect

Atmospheric Research

journal homepage: www.elsevier.com/locate/atmosres

High resolution analysis of rainfall intermittency at mid-latitude using disdrometer decade-long data

Ravi Shankar Pandey [a],*, Alberto Carrassi [a], Federico Porcù [a], Elisa Adirosi [b]

[a] Department of Physics and Astronomy "Augusto Righi", University of Bologna, Viale Berti Pichat 6/2, Bologna, 40127, Emilia-Romagna, Italy
[b] National Research Council, Institute of Atmospheric Sciences and Climate - CNR-ISAC, Via del Fosso del Cavaliere, 100, Rome, 00133, Italy

ARTICLE INFO

Dataset link: https://doi.org/10.5281/zenodo.7708563, https://doi.org/10.5281/zenodo.11102745

Keywords:
Minimum inter-event times
Mass-weighted mean diameter
Stratiform precipitation
Convective precipitation
Intermittency fraction
Wet spell
Dry spell
Intra-event rainfall intermittency
Time averaged rainfall intermittency

ABSTRACT

This study analyzes rainfall structure using an unusually long record of continuous 1-minute disdrometer observations, comprising 11 years (2013–2023) of data from a Thies Clima disdrometer near Rome, Italy. We identify rainfall events based on minimum inter-event times (MITs), calculating rain rate, mass-weighted mean diameter (D_m), as well as stratiform and convective precipitation classification. After cleaning erroneous data, seasonal analysis shows autumn had the highest rainfall with the majority of medium sized drops, winter featured prolonged light rain with smaller drops, while summer recorded the least rainfall but with the highest intensity and largest drops. The differences in drop sizes and rain types across seasons are crucial, as stratiform clouds, linked to steady rain, were more common in autumn and winter, whereas convective clouds, associated with intense, short-duration rain, dominated summer. The study focuses on rainfall intermittency, defined by the abrupt onset or interruptions of rainfall events. Intermittency was measured using the intermittency fraction (IFr), which indicates the proportion of dry time within a given period. Time Averaged Rainfall Intermittency (TARI) estimates IFr over fixed intervals, while Intra-Event Rainfall Intermittency (IERI) does so dynamically between consecutive fixed-length dry periods, also called MIT. Both methods, applied across multiple categories, produced consistent results, validating each other. A diurnal analysis of IFr (15-minute TARI-based) reveals significant seasonal differences, peaking between 9 AM and 2 PM. In summer, sharp peaks occur before noon, followed by a rapid decline in the afternoon, whereas winter maintains a more consistent IFr throughout the day. These seasonal differences remain robust with increasing durations in TARI from 15-minutes to 1 day. Overall, the longest wet spell lasted 19.4 h, while the longest dry spell was 534.4 h. IERI across various MITs shows higher IFr values at shorter MITs, particularly during the summer. These results highlight disdrometers' vital necessity during hazard-prone seasons, causing flash floods and erosion.

1. Introduction

The United Nations water policy report highlights that the global climate change is inextricably linked to water crises associated with extreme weather events (UN-Water, 2019). In particular, short-duration, high-intensity rainfall has been observed more frequently, potentially linked to the effects of global warming (Dunkerley, 2021). Similar increases in the intensity and frequency of extreme weather systems have been reported in studies of tropical cyclones, suggesting a broader response of precipitation-producing systems to ongoing climate change (Pandey and Liou, 2022, 2020). Simultaneously, rapid urbanization driven by population growth exerts immense pressure on existing infrastructure, leading to city expansion without adequate modifications to old drainage systems. Thus, it becomes imperative to monitor rainfall intensity with high accuracy and high resolution, enabling government agencies to update drainage systems effectively and mitigate flooding, landslides, erosion, and flash floods (Zhao et al., 2023; Hassan et al., 2022). In order to enhance our understanding of precipitation and ensure the provision of precipitation products that are more accurate and reliable, it is necessary to consider not only the measurement of precipitation amount and rate, but also its additional physical attributes, such as its microphysical structure, as well as its spatial and temporal properties.

One of the main temporal characteristics of precipitation is intermittency, defined as the occurrence of dry periods within rain events (Dunkerley, 2015). Since rain is intermittent, with long periods without rainfall, many hydrological and meteorological applications use the concept of "rainfall events" (Dunkerley, 2012). Characterizing intermittency is crucial for supporting studies of long-term changes in rainfall intensity (Dunkerley, 2021). Minimum Inter-Event Time

* Corresponding author.
E-mail addresses: ravishankar.pandey@unibo.it, drravi300593@gmail.com (R.S. Pandey).

https://doi.org/10.1016/j.atmosres.2026.109135
Received 24 September 2025; Received in revised form 13 May 2026; Accepted 1 June 2026
Available online 6 June 2026

(MIT) is widely used to distinguish consecutive rain events, preventing overestimation of rainfall statistics (Dunkerley, 2012; Tu et al., 2023). Time-Averaged Rainfall Intermittency (TARI) provides insights into the temporal variability of precipitation over fixed durations, improving hydrological assessments (Dunkerley, 2012). Intra-Event Rainfall Intermittency (IERI) captures fluctuations within individual rain events, highlighting variations in intensity and contributing to the accurate estimation of runoff and flood risks (Dunkerley, 2021).

High-resolution rainfall data from Australia and southern China reveal significant sub-daily rainfall intermittency when analyzed using both time-aggregated and event-based approaches. In the Australian context, TARI based on 1-hour aggregation durations showed intermittency levels of 42%–47%, while TARI and IERI both derived from unaggregated inter-tip times, exhibited higher intermittency of 62%–67% (Dunkerley, 2021). Similarly, in southern China, MIT-based rainfall event analysis showed that IERI increased as event duration decreased, with short-duration events (less than 5 h) exhibiting intermittency exceeding 60%. Higher intermittency was observed during the pre-flood season compared to the post-flood season (Tu et al., 2023). These findings emphasize the highly fragmented nature of rainfall at fine scales and the necessity of including intermittency metrics in hydrological and climate modeling frameworks.

Beyond rainfall intermittency, intermittency frequency is another crucial factor influencing precipitation analysis (Dunkerley, 2021). Defined as the number of interruptions within a rain event, this parameter offers additional insights into rain event structures and potential flood risks (Dunkerley, 2012). Incorporating both intermittency and its frequency provide a more comprehensive perspective on rainfall characteristics, particularly in a changing climate (Sharma et al., 2009; Ulbrich and Atlas, 2007). In Dunkerley et al. (2021), a rain event is defined as rainfall separated by less than 6 h of no rain (6-hour MIT). Within events, the intermittency frequency was found to range from 5 to over 20 interruptions per event. This highlights a highly fragmented rainfall structure, independent of total intermittency duration, and is critical for understanding sub-event rainfall dynamics. Understanding the environmental conditions associated with rainfall variability is particularly relevant because atmospheric and oceanic factors have been shown to strongly modulate the occurrence and intensity of extreme weather systems across multiple temporal scales Pandey (2022).

The aim of the present study is to set up a comprehensive framework to quantify temporal variability of liquid precipitation at different scales, starting from the shortest one (1 min). The investigation of precipitation variability across multiple temporal scales complements previous studies focused on large-scale atmospheric variability, storm climatology, and changes in extreme weather characteristics under changing climatic conditions Pandey and Liou (2020, 2022). To this end, an 11-year disdrometric database collected close to the city of Rome (Italy) is used, exploiting the capability of the disdrometer to provide 1-minute measurements of the rainfall Drop Size Distribution (DSD). Since the main focus of the work is to study the temporal features of the precipitation rate, the disdrometer data are mainly used to compute high-resolution rainrate.

The Thies CLIMA disdrometer (TCD hereafter) is one of the 22 instruments belonging to the disdrometric network fostered by the Italian Group of Disdrometry (GID) (Adirosi et al., 2023a), and provided quasi-continuous DSD measurements over the period 2013–2023. The time frame was not long enough to allow the assessment of climatic trends, however, it allows us to adopt a seasonal perspective to assess rainfall intermittency and its frequency across different time frames. Seasonal variations in rainfall intermittency play a fundamental role in shaping hydrological responses (Caracciolo et al., 2014). Seasonal dependence is a common feature of atmospheric processes and extreme weather phenomena, reflecting variations in thermodynamic and dynamic environmental conditions throughout the year Pandey et al. (2021). Winter rainfall, though prolonged, is typically less intense, whereas summer precipitation exhibits high-intensity, short-duration events with substantial intermittency (Han and Braun, 2021).

The paper is structured as follows: Section 2 describes the data sources, including details of the TCD. Section 3 outlines the methodology employed for measuring rainfall intermittency and key precipitation parameters. Section 4 presents a detailed discussion of seasonal rainfall patterns, and intermittency characteristics. Finally, Section 5 concludes the study by summarizing key findings and their implications for hydro-meteorological risk assessment.

2. Data

2.1. Data source

We used precipitation data from 2013 to 2023 collected from the TCD, installed in Rome (41.8425° N, 12.6464° E) at 102 meter a.s.l.. TCD is a Laser Precipitation Monitors with a measuring area of 45.6 cm^2 and 1-minute temporal resolution. It collects a 22-diameter size by 20-fall velocity matrix with a droplet diameter class range from 0.125 to 8 mm and a fall velocity range from 0.2 to 10 m/s https://www.thiesclima.com/db/dnl/5.4110.xx.x00_Laser_Precipitation_Monitor_eng.pdf. Disdrometers can measure terminal velocity; however, strong winds may cause swirled drops, significantly altering the readings (Capozzi et al., 2021; Friedrich et al., 2013b). Marginal fallers small drops with abnormally high velocities can result from partial sampling of large drops or wind-induced splash/swirl effects (Chatterjee et al., 2022; Friedrich et al., 2013b,a; Yuter et al., 2006). In order to obtain more reliable and accurate Drop Size Distribution (DSD), the raw disdrometer data has been processed. The main steps of the processing are the application of a filter criterion based on the diameter-fall velocity relation to remove spurious drops and the use of a theoretical diameter-fall-velocity relation to compute the DSD (Gunn and Kinzer, 1949). The latter is the (Atlas et al., 1973) relation modified to take into account the terrain height of the disdrometer installation site (Porcù et al., 2014). In the present study, the air density at sea level (1.213 kg/m^3) and at the Rome's disdrometer's station height (1.224 kg/m^3 at 102 meter height), respectively, based on the ISO model (International Organization for Standardization, 1975). Several recent studies have calculated the terminal velocity of raindrops based on their diameter, as provided by the disdrometer (Hauser et al., 1984; Jaffrain and Berne, 2011; Thurai and Bringi, 2005; Tokay et al., 2001).

The disdrometer in Rome is one of the 25 disdrometers currently installed as a part of the Italian Group of Disdrometry (GID, established in 2021). Among its three available data versions, the current study uses version 2 and version 3 that supersede version 1 for the DSD computation by using the diameter-fall velocity relation that takes into account the terrain height of the disdrometer installation site (Adirosi et al., 2023a).

2.2. Data preparations

Measuring accurate period of rain and no-rain is crucial for getting reliable results in rainfall intermittency-based studies. The following are the three main definitions adopted in the current study:

(a) Rain threshold θ: to minimize possible noise created by tiny fog droplets or other spurious signals, we use a rainfall threshold (θ) of 0.01 mm/h for each 1-minute rain data sample. Any recorded minute with rain rate less than θ will be considered as no-rain (Chatterjee et al., 2022; Tokay et al., 2017). Note that θ is usually 0.2 mm/h for rainfall data recorded by the conventional TBRG as their bucket size is 0.2 mm (Dunkerley, 2015; Peters et al., 2010).

As laser-based disdrometers measure individual hydrometeors directly and are therefore capable of detecting much weaker rainfall, with reduced susceptibility to evaporation losses and wetting effects commonly associated with funnel-based gauges. Consequently, lower

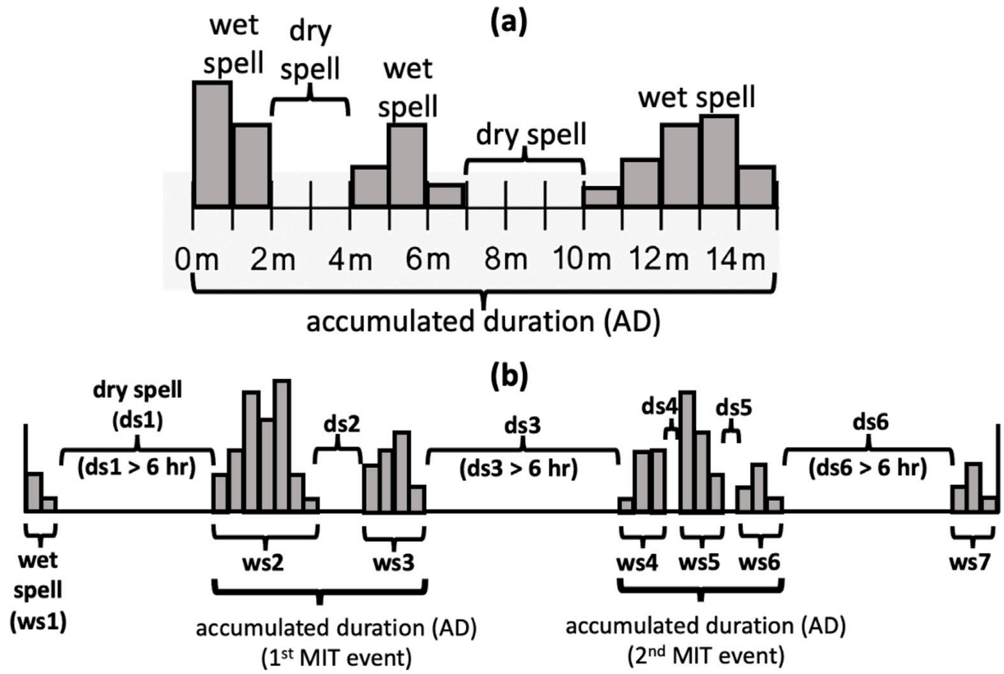

Fig. 1. Diagram showing two alternative methods for defining rain event using (a) fixed accumulated (15-minutes), and (b) minimum inter-event time (6-hours)(MIT) criteria. See text for the explanation.

rainfall thresholds on the order of 0.01 mm h^{-1} have been widely adopted in disdrometer-based studies to distinguish true precipitation from non-precipitating particles or fog (Chatterjee et al., 2022; Tokay et al., 2017). Although rainfall intermittency metrics are sensitive to the choice of θ, the selected threshold lies within the range supported by previous literature and is considered appropriate for the instrument characteristics and temporal resolution used in this study.

(b) Wet and dry spell: based on the formerly defined θ, all continuous recorded data samples with rain rate $\geq \theta$ are called wet spells, while all continuous recorded data minutes with rain rate $< \theta$ are called dry spells.

(c) Rain event: rainfall is a season-dependent, intermittent natural phenomenon, characterized by alternating wet and dry spells until its eventual cessation, followed by an extended dry period (Dunkerley, 2015; Tu et al., 2023). To analyze rainfall systematically, it is essential to establish a clear definition of a rain event. This study considers two definitions:

1. *Fixed Accumulation Criterion* – A rain event is defined as each fixed period of time with at least one minute of rain. We shall consider possible durations of the fixed period ranging between 15 and 1440 min (1 day) (Fig. 1a). This rain event definition is used in Time Averaged Rainfall Intermittency (TARI).
2. *Minimum Inter-event Time (MIT) Criterion* – A rain event is defined as a wet and/or dry spell bounded by two fixed same duration dry spells. These fixed dry spell durations are called the minimum inter-event time (MIT) (Fig. 1b). We tested different durations of the dry spells (between 0.25 to 24 h) to probe the sensitivity of this definition to the length of MIT, and conclusions are drawn based on the most consistent results across different MIT-based classifications. This rain event definition is used in Intra-Event Rainfall Intermittency (IERI).

The dataset contains missing entries due to technical and handling issues, including extreme weather conditions (Adirosi et al., 2023b). To prevent artificial fragmentation of wet and dry spells caused by missing records, all spells immediately preceding or following missing data are removed from the analysis rather than interpolated. This conservative approach ensures that the intermittency metrics are derived only from uninterrupted observations, with the longest wet and dry spells representing lower-bound estimates based on fully observed events.

Furthermore, we broadly classified the data into a few drop-size categories for ease of analysis: raindrops with diameters between 1 mm and 3 mm are classified as mid-sized drops, while drops smaller than 1 mm are considered small, and those larger than 3 mm are categorized as large. This classification is consistent with previous studies (Ganai et al., 2016; Janapati et al., 2020; Seela et al., 2017; Tokay et al., 2008).

3. Methodology

3.1. Techniques for measuring rainfall intermittency

Rainfall intermittency, as defined in this study, refers to interruptions within a continuous rainfall period, either on a fixed time scale (for TARI), or event-based scale (for IERI). These intermittent periods are by construction bounded by rainfall occurrences (Dunkerley, 2021). We use two metrics for quantifying the rainfall intermittency:

(a) Rainfall Intermittency Fraction (IFr): It is the ratio between total duration of dry spells and the accumulated duration (AD), where AD is the fixed period of time over which the rain is measured. In the present study, the unit of the AD, dry and wet spells are minutes.

$$IFr = \frac{AD(I)}{AD}, \tag{1}$$

where $AD(I)$ is the total duration of dry spells. Hence, IFr values ranges from 0 to 1, where "0" means continuous rain without any stoppage and "1" means there is no rain at all during that particular accumulation duration. We ignore IFr values of 1 to avoid counting long dry spells as rainfall intermittency. Intermittency can only be counted if there is the presence of at least two wet spells, each at different sides of the dry spell (Dunkerley, 2021).

(b) Rainfall intermittency frequency: It is the sum of the number of interruptions in rainfall during an AD (Dunkerley, 2021). The first dry spell in the rain must be counted after the first wet spell and the last before the last wet spell during a fixed timeframe or even-based timeframe. Hence, the maximum possible frequency of rainfall intermittency is: $N = \frac{AD}{2} - 1$. Each jump from wet to dry spell is

counted as 1, which starts from the first jump from the wet spell and ends before the last wet spell of the rain event. Rainfall intermittency fraction (IFr) and rainfall intermittency frequency play a crucial role in defining the temporal variability of precipitation, influencing both hydrological responses and atmospheric dynamics (Dunkerley, 2021).

Following the definitions of rainfall intermittency fraction and frequency, along with Fig. 1a, if the accumulated duration (AD) is 15 min, comprising 5 min of dry spells and 10 min of wet spells, the intermittency fraction (IFr) will be 5/15 = 0.33. Whereas the intermittency frequency will be 2, indicating that rainfall ceased twice during the entire AD. Similarly, in Fig. 1b, the intermittency frequency is 1 (i.e., ds2) and 2 (i.e., ds4, ds5), respectively, for MIT-6 h, whereas IFr is 3/14 (or 0.21) and 2/11 (or 0.18), respectively.

3.2. DSD integral parameters

(a) Rain rate: The rain rate can be estimated from the Drop Size Distribution (DSD) data using the 3rd moment. The DSD data, which includes 22 diameter classes with the mean value of each class (D_i), their measured terminal velocity ($v(D_i)$), the number of drops for unit of volume and diameter ($N(D_i)$), and the width of each class (ΔD_i), are sufficient to measure the rain rate (R, in mm per hour) (Adirosi et al., 2023b; Caracciolo et al., 2006):

$$R = 6\pi \times 10^{-4} \sum_{i=1}^{22} v(D_i) D_i^3 N(D_i) \Delta D_i. \quad (2)$$

(b) Mass-weighted mean diameter; Dm: The mass-weighted mean diameter (D_m) is the ratio of the 4th and 3rd moments of the DSD. It is a characteristic parameter of the DSD (Han and Braun, 2021), and represents the average size of rain drops weighted by mass (Seto et al., 2013; Williams et al., 2014; Wood et al., 2013). It is directly proportional to the rain rate (Zeng et al., 2022), and D_m values are highest for convective clouds, particularly during summer over land. Tropical zones exhibit larger D_m values and higher standard deviations. Additionally, large convective D_m values are observed at high latitudes, where intense convection and ice layers contribute to the largest D_m values (Han and Braun, 2021).

3.3. Precipitation classification

Disdrometers classify precipitation using drop diameter, terminal velocity, and air temperature. However, measuring solid precipitation is challenging due to variable ice density/shape affecting velocity-size relations (Gunn and Kinzer, 1949) and instrumental biases causing classification errors (Angeloni et al., 2024; Fehlmann et al., 2020). To ensure accuracy, we exclude full disdrometer-based precipitation classifications but rely on DSD data for distinguishing stratiform and convective precipitation.

Stratiform and convective precipitation represent two primary categories of rainfall, distinguished by their driving physical mechanisms, and several classifications are present in the literature, based on DSD (Caracciolo et al., 2006) or rain rate properties (Bringi et al., 2003). According to the criterion by Bringi et al. (2003), precipitation is convective if the standard deviation of rain rates is ≥ 1.5 mm h^{-1}; otherwise, it is classified as stratiform. Building on this framework, Chen et al. (2013) and Zeng et al. (2022) proposed a refined classification. They determined that for at least 10 consecutive 1-minute rainfall samples, precipitation qualifies as stratiform if the rain rate R exceeds 0.5 mm h^{-1} with a standard deviation of R ≤ 1.5 mm h^{-1}. Conversely, it is identified as convective if R is ≥ 5 mm h^{-1} and the standard deviation of R exceeds 1.5 mm h^{-1}. Rainfall samples failing to meet these criteria are excluded from classification. This study adopts the aforementioned fixed criteria of detecting precipitation types delineated by Bringi et al. (2003), Chen et al. (2013), and Zeng et al. (2022).

It should be noted that precipitation classification based solely on rain-rate thresholds, as adopted here, has inherent limitations. Previous studies have shown that weak or shallow convective precipitation can exhibit rain rates comparable to stratiform rain, leading to potential misclassification when intensity alone is used (Bringi et al., 2003). Disdrometer-based analyses have demonstrated that incorporating drop size distribution (DSD) properties (e.g., D_m, N_w) provides a more physically meaningful separation of convective and stratiform regimes, particularly for weak convection (Bringi et al., 2003; Tokay et al., 2001). Nevertheless, the rain-rate-based classification adopted in this study follows well-established criteria widely used in the literature, originally proposed by Bringi et al. (2003) and subsequently applied and refined in more recent studies (Chen et al., 2013; Zeng et al., 2022). This choice ensures methodological consistency and facilitates comparison with previous studies. While a DSD-based classification may offer improved physical discrimination, its robust and consistent application over the long-term, high-resolution datasets would require a dedicated analysis and introduce additional uncertainties, and was therefore beyond the scope of the present study.

4. Results and discussion

4.1. Seasonal precipitation characteristics

Approximately 16.3% (13,515 h) and 15.9% (13,183 h) of the total recorded data were excluded from the present study as they were categorized as missing and removed data, respectively. Due to the non-continuous nature of data recording, the available dataset is not suitable for year-wise comparisons.

Rome records rainfall for 4.8% of the total recorded duration (3983 h out of 82,893 h), accumulating 8190.2 mm of rainfall over the 11-year study period (2013–2023). The low percentage of rainy minutes can be partially due to the missing and removed data, but it is primarily due to the nature of the precipitation. In other words, if we consider a dataset with no missing minutes, we will have a similar percentage of rainfall minutes. Notably, this is one of the longest available disdrometer datasets for a single location. In 2014, the highest recorded rainy duration was 464.2 h (28.2% more than the yearly mean of 362.1 h), whereas 2013 had the lowest recorded rainy duration of 279.9 h (22.7% less than the yearly mean). Over the entire study period, the average rain amount per rainy minute, excluding all dry minutes, was 0.034 mm, the average rain rate was around 2 mm/h.

Summer experiences the highest rain rate (3.4 mm/h), though it records the lowest total rainfall (1329.6 mm) (Fig. 2). In contrast, winter has the longest rainfall duration but lower total accumulation than autumn due to a higher proportion of small drops. Autumn, which has the highest proportion of medium-sized drops, records the greatest total rainfall (3126.8 mm), 1.57 times more than winter. Seasonal differences are further confirmed by the average mass-weighted mean diameter: D_m, with the largest drops in summer (1.39 mm) and the smallest in winter (0.98 mm).

Fig. 3 shows DSD categorized by stratiform and convective precipitation in different seasons. The Figure reveals several crucial points: (i) convective precipitation drops are larger and show more seasonal variations than stratiform precipitation; (ii) the number of drops per unit of volume is one order of magnitude larger for convective than for stratiform rain; (iii) summer possesses the largest drop size in general, shown by the green dashed line, than other seasons during convective precipitation; (iv) convective rain is characterized by very large hydrometeors. The presence of a relative peak in the convective DSD across all seasons is difficult to explain: a possible reason is the contamination by solid/melting hydrometeors. A close inspection of the database shows that, out of the 1720 total minutes with drops larger than 6 mm, 1654 are classified as "solid" by the TC algorithm of particle classification. For these minutes, we expect that the retrieval of rain rate is more uncertain. Their impact on our results is negligible given that the discrimination between wet/dry spells is not influenced by the particles' habits.

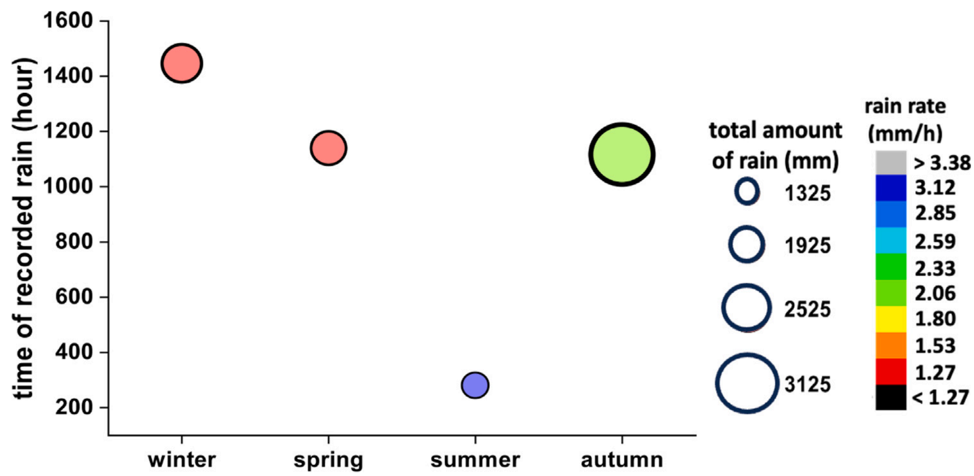

Fig. 2. Rain period, total amount of rain, and rain rate in different seasons during 11 years of study period.

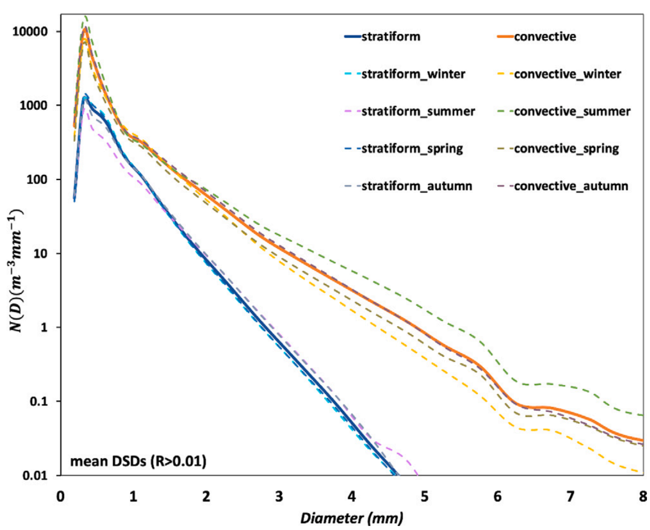

Fig. 3. Drop size distribution of rain caused by stratiform and convective clouds during the study period and in various seasons.

Table 1
Statistics related to wet and dry spells during 2013 to 2023 in Rome based on TCD data.

	Wet spell duration (min.)	Rain amount (mm)	Avg. rain rate (mm/h)	Dry spell duration (min.)
max.	1162	149.1	37.0	32 062
avg.	14.1	0.48	0.59	234.6
total	238 961	8190.2	–	3 943 682
st. dev.	38.9	2.95	1.78	1217.6

4.2. Wet and dry spells

Table 1 provides the statistics of wet/dry spells and overall rainfall during 2013 to 2023 in Rome using the Thies Clima disdrometer.

The longest recorded wet spell lasted 19.4 h, whereas the longest period without rain lasted 534.4 h (more than 22 days). Note the estimate of the longest dry or wet spell can be affected by breaks caused by missing and/or removed data result in as an underestimation. Overall, 16,940 wet spells (winter: 1162, spring: 4534, summer: 1359, autumn: 4766) and 16,810 dry spells (winter: 6264, spring: 4513, summer: 1322, autumn: 4741) were recorded during the study period. Hence, the majority of wet spells are in autumn, whereas winter rain is characterized by the least wet spells but with the longest average duration. Overall, a similar number of wet and dry spells were recorded during the study, with seasonal variations in their frequency. Only wet spells that fully occur within a season are counted for that season.

Fig. 4 shows the number of occurrences and the linear fit for wet and dry spells, in a log–log plane. Fig. 4 shows that straight line fitting is almost suitable to fit all wet (with 57-degree slope) and significant (94% of data or up to 12 h) dry spells (with 52-degree slope) frequency patterns. Both dry and wet spells are well distributed as power low but with the right end of the distributions slightly deviate, due to the rare occurrence of very long spells. It can deviate largely for dry spell more than 12 h failing the power law fit; in fact, the highest duration even goes up to 534 h. Deviations from the power-law suggest different governing processes (e.g., weather systems, geography, or seasonality) for longer dry periods.

In Fig. 4, R^2 is in both cases close to 1 indicating good power-law fit, whereas RMSE nearby 0.2 indicates low prediction error. Hence, both values ensuring the good quality of fit. Higher angle in wet spells shows the fast declining of continuous precipitation with time.

A first inspection of Fig. 4 immediately reveals that both wet and dry spell durations exhibit scale-free, power-law behavior, indicating long-range temporal correlations in rainfall intermittency, with dry spells showing stronger persistence than wet spells. More specifically the duration of wet spells follows a power-law distribution with exponent, $\alpha_{wet} \approx -1.54$: short wet spells are very common, but long wet spells are rare, with no obvious characteristic timescale. This suggests scale-free behavior: rainfall persistence does not have a preferred duration over the observed range, and it is typical of intermittent, clustered rainfall, often associated with convective processes, self-organized or correlated atmospheric dynamics. Dry spell durations also follow a power law, but with a shallower exponent, $\alpha_{dry} \approx -1.30$: long dry spells are relatively more frequent than long wet spells. Dry spells dominate long-time persistence, while wet spells are more fragmented. Dry periods are more persistent and more likely to last longer than wet periods. This asymmetry is very typical in rainfall statistics and reflects large-scale subsidence, stability, or blocking patterns: atmosphere tends to “stay dry” longer than it “stays wet”. We choose to apply the cutoff at 720 min to avoids regime mixing: e.g. synoptic-scale droughts vs short dry breaks. In a scale-invariant system, such behavior implies that the probability distributions follow a power-law over a range of temporal scales, appearing approximately linear in log–log space, and that no single characteristic time scale dominates the occurrence of wet or dry intervals. A similar rainfall interruption mechanisms operate across multiple temporal scales, from minutes to several hours or days. The deviations from power-law behavior at longer dry-spell durations, visible as curvature or breaks in the tail of the distribution, imply a breakdown of scale invariance and reflect the increasing influence of different controlling processes, such as persistent synoptic-scale circulation patterns,

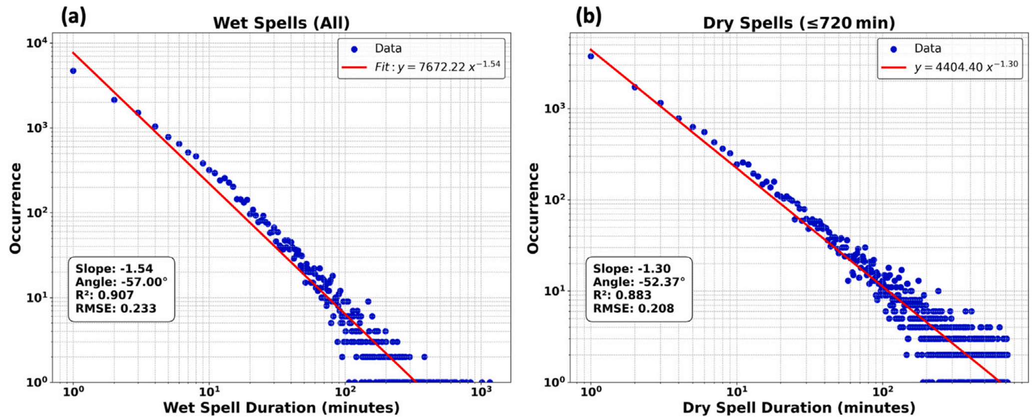

Fig. 4. (a) Number of wet spell and (b) dry spell occurrences and their respective straight line fittings.

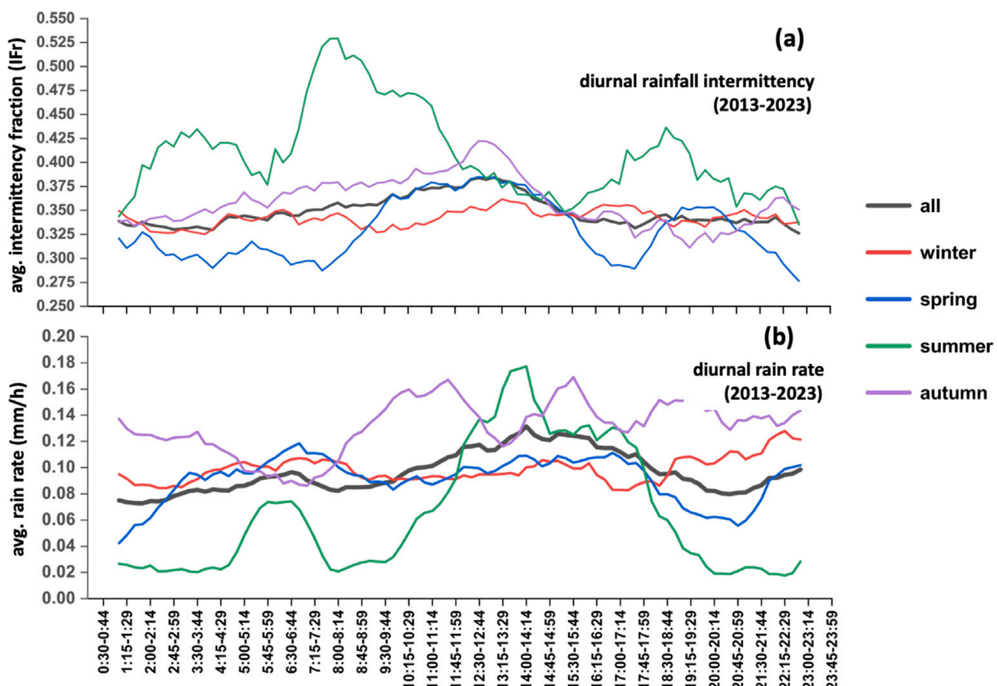

Fig. 5. Diurnal variation in (a) rainfall intermittency and (b) rain rate using AD 15-minutes and a 9-step moving average during 2013–2023 in Rome. Note that rain rate is averaged over all samples, including also completely dry ADs.

seasonal atmospheric stability, and large-scale climatic forcing. These departures from ideal scale-invariant behavior highlight the coexistence of multiscale rainfall intermittency with regime-dependent atmospheric controls.

4.3. Rainfall intermittency

4.3.1. Time Averaged Rainfall Intermittency (TARI)

A rain event can be analyzed by fixing the Accumulated Duration (AD) (Dunkerley, 2012). Here we take 15-minute, 30-minute, 60-minute, and 1440-minutes AD values. Hence, TARI is defined as the value of the intermittency fraction (IFr) measured using Eq. (1) for the fixed accumulated duration (AD) with at least one minute of rain.

To achieve the best resolution for assessing the diurnal variations of rainfall intermittency, 15-minute AD (rain parameters also will be averaged for each 15-minute period) is chosen in the current study, along with a 9-step moving average for smoothening (Fig. 5).

First, we note that the diurnal dynamic of the annual curve is low, between 0.325 (night and afternoon) and 0.385 (noon), while the seasonal curves show clearer signals (Fig. 5a). The most pronounced diurnal rainfall intermittency dynamics is shown for summer (green curves): the IF has three wide peaks (around 3AM, 8AM, and 7PM). All peaks are found in hours with lowest averaged rainfall rates (Fig. 5b), while low intermittency characterizes the rainfall rate peaks. This indicates that weak precipitation in summer is prone to intermittency, while heavy rainfall tends to be more continuous. This behavior is still present, although less pronounced, for spring (blue curves) with weak intermittency peaks around midday and late afternoon corresponding to slightly lower rainrates. Winter and autumn show again very little dynamics and almost no correlation to rainfall rate. In summary, Fig. 5 indicates that, in general, intermittency depends on the season and the time of the day, with stronger dependence in summer.

Fig. 6 shows the average intermittency fraction and frequency values for different seasons across different time-averaged frameworks.

The TARI, quantified using the intermittency fraction and with the mean intermittency frequency, exhibits a consistent decline as the temporal resolution decreases from a daily scale to 60-minute, 30-minute, and ultimately 15-minute intervals (Fig. 6). The TARI values peak in

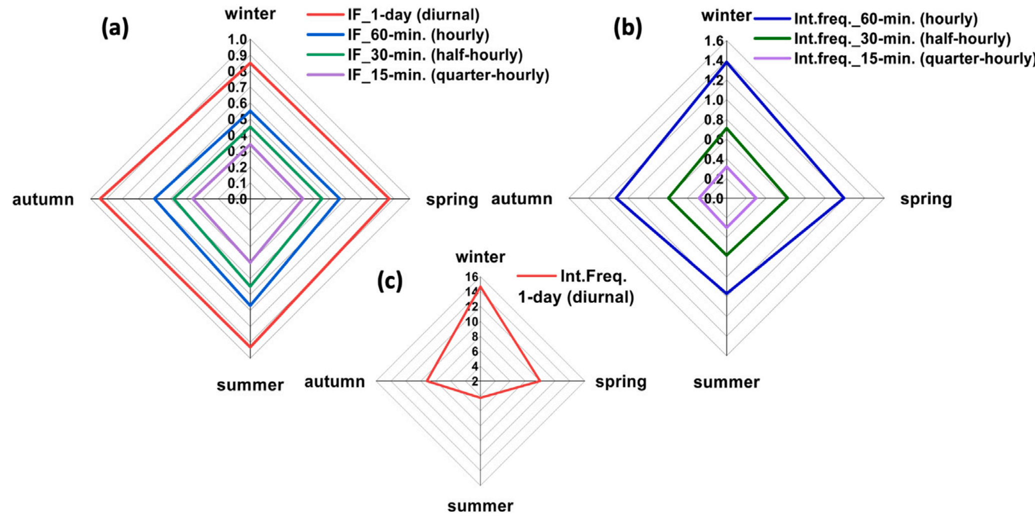

Fig. 6. Averaged rainfall (a) intermittency fraction and (b, c) intermittency frequency in various seasons for 15-min., 30-min., 1-hour, and 1-day averaged timeframes for whole study period of 2013–2023.

summer and are lowest in winter (Fig. 6a), while rainfall frequency follows the opposite trend (Fig. 6b, c). Winter rain is more frequent but less intense, with minimal stoppages, whereas summer rain has fewer but longer interruptions, leading to higher intensity (Fig. 6b, c). This makes summer more prone to flash floods and flooding, posing ecohydrological challenges. A recent research also validates it and shows that TARI varied with aggregation duration (AD): 1-hour AD data showed lower intermittency levels (42%–47%), whereas unaggregated inter-tip time (ITT) data revealed higher intermittency (62%–67%) for both daily and event-based analyses (Dunkerley, 2021).

4.3.2. Intra-Event Rainfall Intermittency (IERI)

Rainfall is a sporadic natural process that typically occurs in clusters or bursts, with distinct onset and cessation marked by rain-free intervals of a predefined duration, known as the Minimum Inter-Event Time (MIT) (Dunkerley, 2015). The constant MIT criterion is a widely adopted approach for distinguishing independent rainfall events within continuous precipitation records (Tu et al., 2023). Accurately defining a rainfall event is a critical aspect of hydrological research worldwide (Dunkerley, 2012, 2015; Tu et al., 2023). A well-defined rainfall event classification is essential for analyzing its impact on runoff generation and soil erosion processes (Tu et al., 2023).

A 6-hour MIT is widely used in hydrology and soil erosion research to define rainfall events, ensuring rainless intervals of at least six hours before and after an event (Dunkerley, 2015; Huff, 1967; Meng and Wang, 2016). However, MIT values vary by climate and geography, influencing rainfall kinetic energy, intensity, and erosivity (Caracciolo et al., 2012; Tu et al., 2023). Studies have identified optimal MIT values, such as 4 h in China based on rainfall erosivity (Tu et al., 2023), while meteorological research often uses shorter MITs (e.g., 2 h) (Guo and Urbonas, 2002). Given this variability, this study employs ten MIT values ($\frac{1}{4}$ to 24 h) to delineate rainfall events, distinguishing rain and no-rain periods based on rainfall rates below 0.01 mm/h. Intra-Event Rainfall Intermittency (IERI) is quantified using the IFr, calculated both per event and across MIT values to ensure consistency and minimize bias (Dunkerley, 2012). A recent research shows that based on inter-tip time (ITT) analysis, IERI values ranged from 62%–67% across daily and event-based scales. This reflects a high proportion of rainless periods within events, even during intense rainfall. IERI captures the true intermittency of rainfall better than aggregated approaches, emphasizing its utility in sub-daily hydrological modeling (Dunkerley, 2021). Events defined using a 24-hour MIT had an average of 49.4 h of contiguous no-rain time, approximately six times the contiguous rain duration (6.2 h). This ratio increased to nearly eight times for a 6-hour MIT (25.6 h no-rain vs. 2.9 h rain) and continued rising as MIT decreased. The longest wet spell declined from 1.6 h (24-hour MIT) to 1.1 h (6-hour MIT).

Most parameters exhibit low sensitivity to changing MIT, with the notable exception of the average rain rate per event, which reached a maximum value of 29.2 mm/h at an MIT of about 5 h and decreased for both shorter and longer intervals. Similar sensitivity of event-based rainfall intensity to the choice of MIT has been reported in previous studies (e.g., Tu et al., 2023), where short MITs tend to merge physically distinct precipitation pulses and dilute event intensity, while long MITs can fragment coherent storm systems, leading to reduced mean event intensities. The presence of a local maximum in average event rain rate at intermediate MITs (5 h) has therefore been interpreted as a supporting indicator of a physically reasonable event definition, rather than a definitive criterion for MIT optimality. Hence, based on the above discussion, an MIT of 5–6 h for defining rainfall events in Rome is used hereafter.

However, as emphasized in hydrological and ecohydrological studies (Huff, 1967; Meng and Wang, 2016; Caracciolo et al., 2012; Guo and Urbonas, 2002), variations in rainfall intensity alone are insufficient to conclusively identify an optimal MIT. Robust determination, independent from the event, requires complementary information on soil moisture dynamics, runoff response, and land–surface processes. Multiple MIT values were examined in this study in order to assess the sensitivity of the derived rainfall metrics to the event-definition criterion and to ensure that the main results are robust across a reasonable range of MIT choices. The identification of a physically optimal MIT, however, requires dedicated soil-moisture-based experimentation and therefore remains beyond the scope of the present analysis.

Figs. 7 and 8 present the variations in several studied parameters across different seasons for changing MIT durations. Results can be summarized as follow:

Due to the intrinsic event-to-event variability driven by the intermittent nature of the processes and the co-existence of multiple rainfall regimes, the standard deviations of the quantities in Figs. 7 and 8 range around and sometimes exceeding the averages values displayed in the figures. For the sake of readability, they are not shown.

- **Winter** is characterized by the longest rainfall durations (Fig. 8d) and the highest frequency of interruptions (Fig. 7b), indicating frequent fragmentation of precipitation. At the event scale, winter exhibits the lowest intra-event rainfall intermittency (IERI; Fig. 7a), indicating that rainfall events are internally more continuous, with smaller dry interruptions once an event is defined.

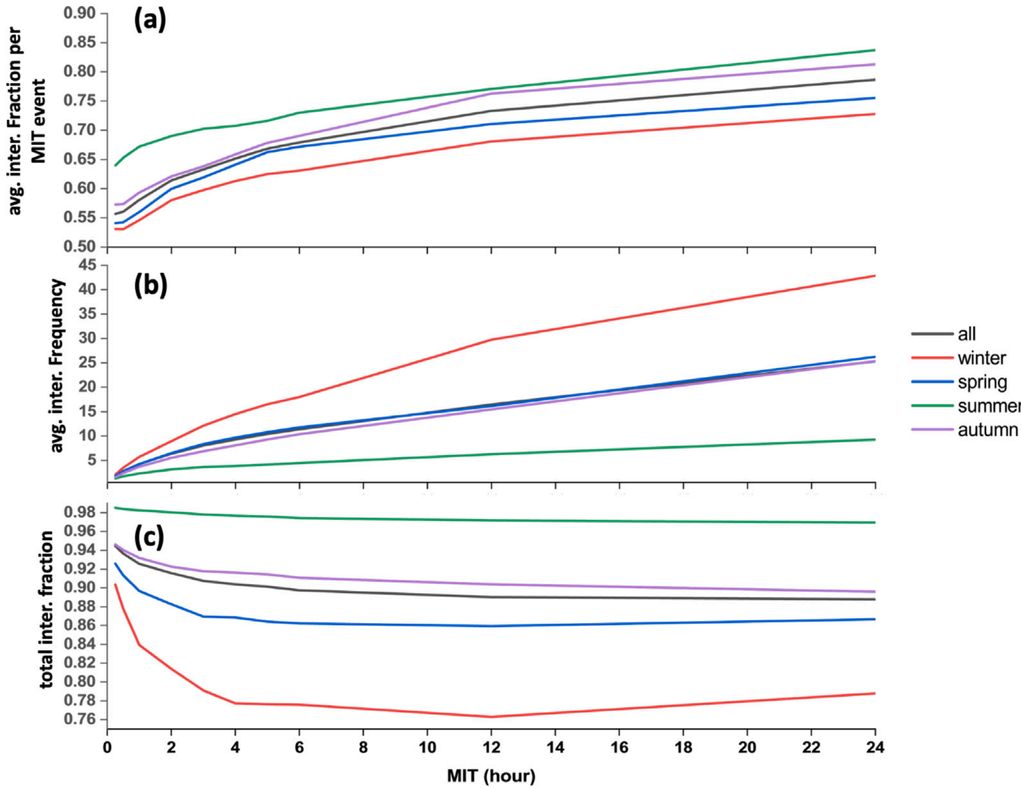

Fig. 7. Variation in (a) average intermittency fraction, (b) average intermittency frequency, and (c) total intermittency fraction with varying MIT cases along with their seasonal fluctuations. Note that the total intermittency fraction is computed as the ratio of the total dry-time duration to the total recorded duration for a given MIT definition, whereas the average intermittency fraction is obtained by first computing the intermittency fraction (IFr) for each individual rainfall event and then averaging these values for the same MIT definition.

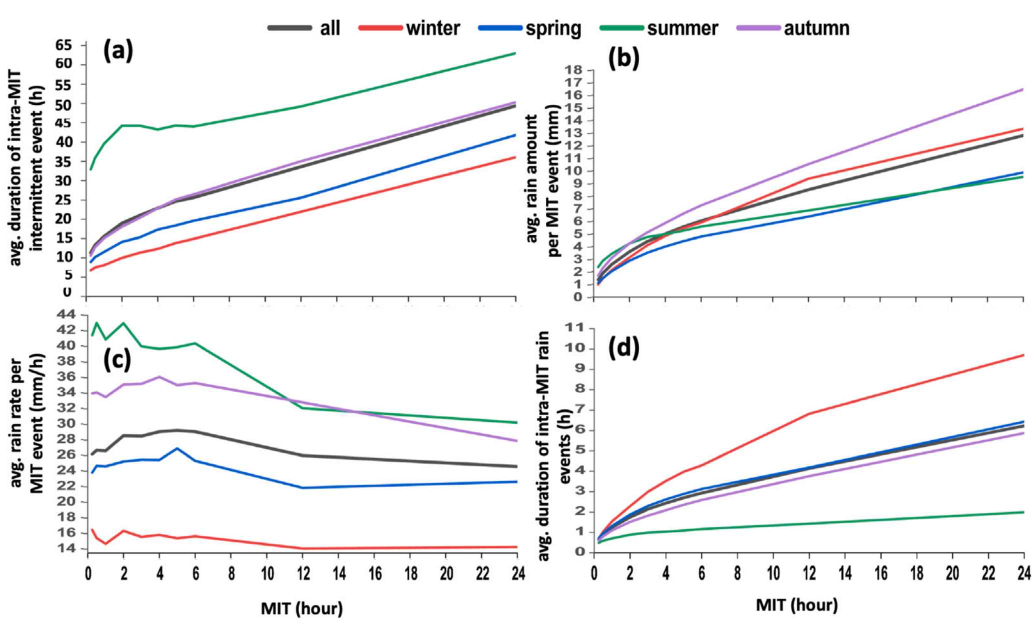

Fig. 8. Variation in (a) average rainfall duration of intra-MIT intermittent event (hour), (b) average rain amount per MIT event (mm), (c) average rain rate per MIT event (mm/h), and (d) average duration of intra-MIT rain events (hour) with varying MIT cases along with their seasonal fluctuations.

This behavior is consistent with the seasonally aggregated intermittency shown in Fig. 7c, where winter also exhibits the lowest total intermittency, indicating that dry periods make the smallest contribution to the overall time span when all MIT-defined rainfall events are considered collectively. It is important to note that Fig. 7a quantifies intermittency at the individual event scale by averaging the fraction of dry time within each MIT-defined rainfall event, whereas Fig. 7c provides a complementary, season-integrated measure obtained by aggregating all dry and wet periods across the entire season, independent of individual event boundaries. In addition, winter shows the lowest rain intensity (Fig. 8c) and low mean rainfall per rainy minute (Fig. 8a).

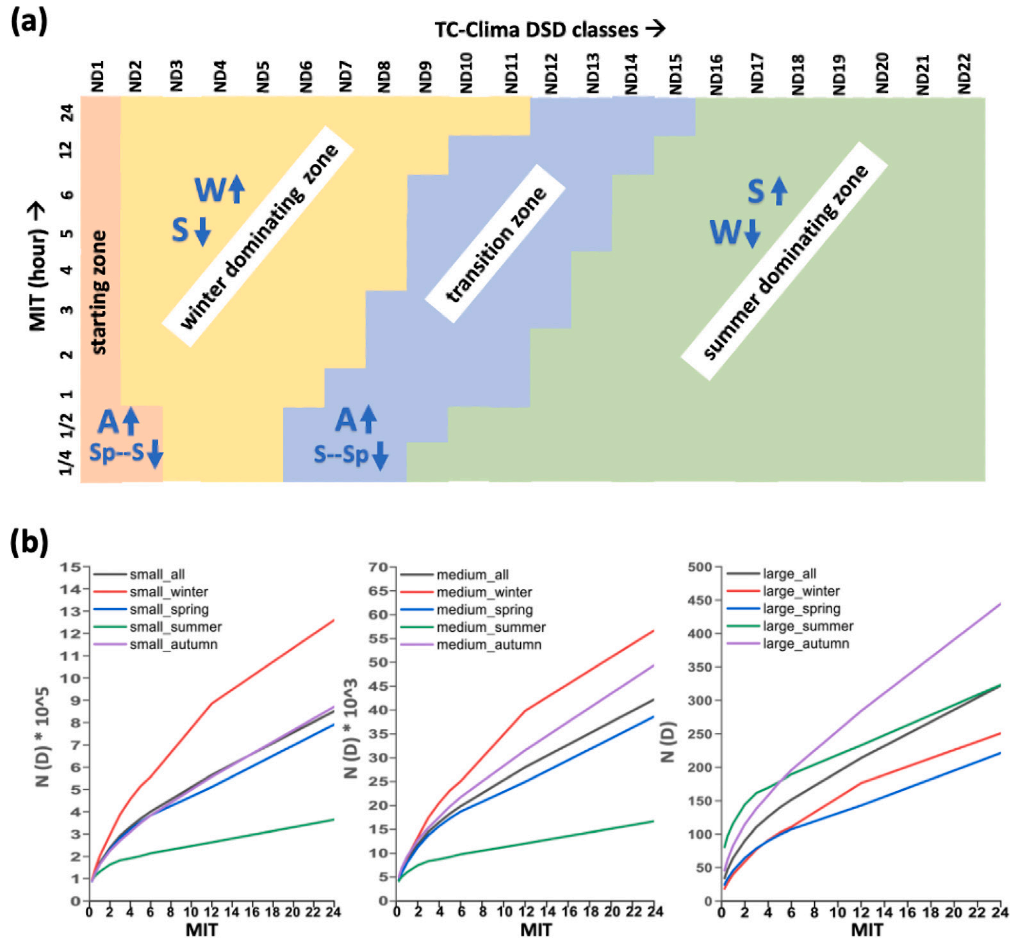

Fig. 9. Classification of (a) zones based on domination of different seasons with varying droplet sizes in different MIT cases, and (b) drops in small (< 1 mm), medium (1 mm to < 3 mm), and large sizes (>=3 mm) along with their seasonal variations in different MIT cases, and (c) drops with varying diameter in different season and zone for 24 hr, 6 hr and $\frac{1}{4}$ hr MIT cases. Note in 2(c) that with decreasing MIT values (24 hr MIT to $\frac{1}{4}$ hr MIT), the transition zone shifts to lower diameter classes, resulting shrinking winter dominating zone. Also, with decreasing MIT values, the number of drops in all diameter sizes reduces, the contrast between frequency of summer and winter season drops decreases in winter dominating zone and increases in summer dominating zone, respectively.

As a result, despite frequent interruptions, winter precipitation generally poses a relatively low ecohydrological risk.

- **Summer** exhibits the shortest rainfall durations (Fig. 8d) and the lowest total rainfall accumulation (Fig. 8b), but it displays the highest rainfall intermittency at both the event scale (Fig. 7a) and the seasonal scale (Fig. 7c). Summer rainfall is characterized by fewer interruptions (Fig. 7b), yet markedly higher rain intensities (Fig. 8c) and larger mean rainfall per rainy minute (Fig. 8a), consistent with convective dominance. Although summer receives the least cumulative rainfall, the combination of high intermittency and high intensity substantially increases the susceptibility to flash floods, landslides, and soil erosion, making summer the season with the highest ecohydrological risk.
- **Autumn** records the highest total rainfall accumulation (Fig. 8b) and relatively long rainfall durations (Fig. 8d). While autumn shows higher intermittency than winter, it remains consistently less intermittent than summer at both the event scale (Fig. 7a) and the seasonal scale (Fig. 7c). Rain intensities (Fig. 8c) and mean rainfall per rainy minute (Fig. 8a) are generally moderate. Consequently, despite larger accumulated rainfall amounts, autumn presents a lower ecohydrological risk than summer due to its more sustained and less fragmented precipitation structure.

These findings are consistent with previous results showing that winter (summer) exhibits the lowest (highest) average rain amount per rainy minute (0.023 mm vs. 0.079 mm) and the lowest (highest) average rain rate (1.28 mm h^{-1} vs. 3.38 mm h^{-1}). Similarly, winter (summer) displays the lowest (highest) IERI per MIT event (0.63 vs. 0.73 for a 6-hour MIT; Fig. 7a) and the lowest (highest) total intermittency fraction (0.78 vs. 0.97; Fig. 7c). Together, these results highlight that rainfall intermittency and intensity, rather than total accumulation alone, are key controls on seasonal ecohydrological risk.

Further investigation, particularly on DSD correlations, is necessary to enhance the understanding of seasonal rainfall dynamics. A comprehensive DSD analysis for all seasonal rainfall events is presented in Figs. 9 and 10.

In particular, Fig. 10 confirms that a longer MIT increases drop frequency, aligning with Tu et al. (2023), who reported that longer MITs lead to greater depth, duration, and rainfall erosivity, but lower mean intensity. Fig. 9(b) shows that winter has the highest frequency of small (<1 mm) and medium (<3 mm) drops, while summer exhibits the lowest. However, for larger drops (>3 mm), this trend reverses in a transition zone where drop frequency declines in winter and increases in summer.

Based on dominance of different seasons for different drop sizes with varying MITs, the Drop frequency zones are classified as follows:

(a) Starting Zone: Dominated by ND1 drops (0.125 mm–0.25 mm). Autumn has the highest drop frequency, followed by winter, while spring and summer record the lowest.

(b) Winter Dominating Zone (WDZ): Comprising small-to-medium drops, winter has the highest drop frequency, while summer has the lowest.

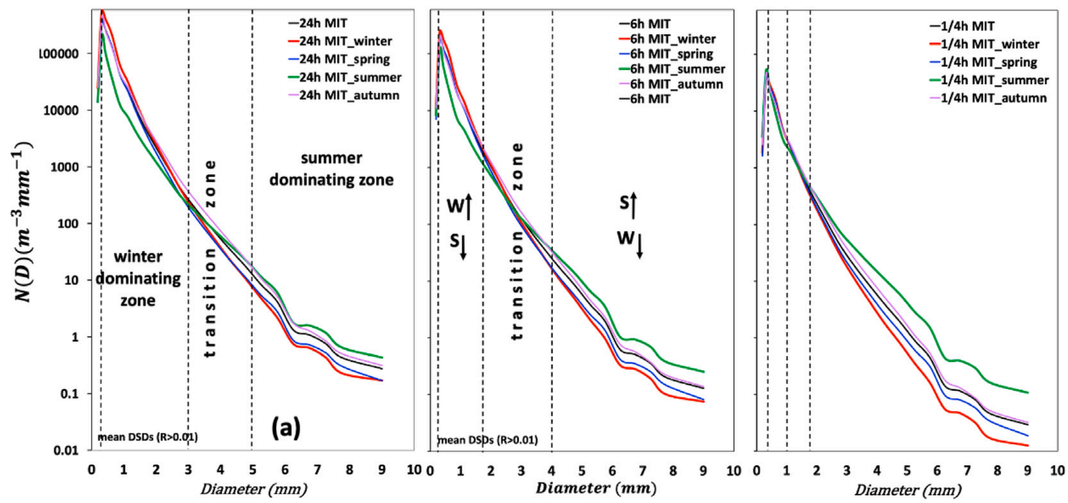

Fig. 10. Classification of drops with varying diameter in different season and zone for (a) 24 hr, (b) 6 hr and (c) $\frac{1}{4}$ hr MIT cases. Note that with the decreasing MIT values (24 hr MIT to $\frac{1}{4}$ hr MIT), the transition zone shifts to lower diameter classes, resulting shrinking winter dominating zone. Also, with decreasing MIT values, the number of drops in all diameter sizes reduces, the contrast between frequency of summer and winter season drops decreases in winter dominating zone and increases in summer dominating zone, respectively.

(c) Transition Zone (TZ): A shift from winter to summer dominance. Drop frequency in winter declines, while it increases in summer.

(d) Summer Dominating Zone (SDZ): Contains the largest drops, with summer contributing the most and winter the least.

Despite the high drop frequency in WDZ, 97.2% are small drops (<1.75 mm), contributing minimally to rain accumulation. Winter, with the lowest rain amount per minute (0.023 mm) and rain rate (1.28 mm/h), poses minimal flood risks. Conversely, SDZ, with fewer but larger drops (≥4 mm), contributes significantly to rainfall intensity. Summer, with the highest rain rate (3.38 mm/h) and intermittency fraction (0.97), is prone to flash floods, landslides, and soil erosion.

Zone-based classification provides deeper seasonal insights than broad droplet size categories, highlighting summer's dominance in large-drop rainfall, which is less evident from Fig. 9b only. This method is crucial for seasonal DSD analysis across varying MIT cases.

4.4. Physical and hydrological interpretation of seasonal and diurnal intermittency patterns

The seasonal variability in rainfall intermittency emerging from our dataset over Rome is patently related to the underlying Mediterranean climate of the region, typified by wet autumn and winter and by dry summer conditions. Mid-latitude frontal systems dominate rainfall during autumn and winter, while summer is usually governed by subtropical anticyclonic conditions that suppress large-scale rain formation, leading to distinct seasonal differences in precipitation frequency and intensity (Weatherspark.com, 2025). Moreover, regional studies show that Mediterranean rainfall can vary strongly both within and among seasons due to large-scale atmospheric variability (Deitch et al., 2017).

Fronts and cyclonic systems associated with winter storms generally produce stratiform rain that persists over hours to days with smaller temporal gaps, resulting in lower intermittency fractions in the cold season. Conversely, summer rainfall in Mediterranean areas tends to be driven by localized instability and convective processes, which produce short-lived, high-intensity showers separated by longer dry intervals—a key behavior leading to high intermittency fractions in summer (Treppiedi et al., 2022). Convective precipitation exhibits strong sub-daily variability and tends to concentrate in the warmer months, even though the total summer accumulation remains lower than in winter (Treppiedi et al., 2022).

Diurnal intermittency patterns reflect thermodynamic drivers of convective activity. In summer, surface heating during the day enhances atmospheric instability, increasing the likelihood of convective rainfall later in the afternoon and evening. This diurnal cycle contributes to the observed peaks in intermittency metrics during specific daytime hours, where rapid onset and decay of convective cells create pronounced temporal gaps in rain occurrence (Treppiedi et al., 2022). In contrast, during autumn and winter, when large scale synoptic forcing is more influential than local surface heating, rainfall is less tied to diurnal heating cycles and thus shows a more subdued daily signal in intermittency patterns (Peña-Angulo et al., 2020).

From a hydrological perspective, rainfall intermittency primarily modulates the temporal distribution of water inputs, rather than directly determining impacts. Short-duration, high-intensity precipitation, occurring in highly intermittent regimes, which is quite common in summer, can temporarily exceed local infiltration capacity, thereby increasing the likelihood of rapid surface runoff generation, particularly in small or urbanized catchments, as documented in previous hydrological studies (Tramblay et al., 2023). In contrast, more persistent and less intermittent precipitation typical of winter seasons tends to promote progressive soil wetting, sustained soil moisture availability, baseflow contribution, and groundwater recharge, even when rainfall intensities are moderate (Tramblay et al., 2023). These contrasting precipitation structures influence runoff response times, soil moisture dynamics, and vegetation water availability across seasons, which are key components of ecohydrological functioning. While the present study does not quantify event-scale impacts such as flash flooding or erosion probabilities, the documented seasonal and diurnal variability in rainfall intermittency provides a physically relevant context for interpreting hydrological sensitivity to precipitation timing in the Mediterranean environments (Serrano-Notivoli et al., 2022).

Finally, beyond the aforementioned seasonal and diurnal cycles, previous studies have also linked the Mediterranean region's precipitation variability to complex interactions between atmospheric circulation patterns, including such teleconnections as the Western Mediterranean Oscillation (WeMO) and Mediterranean Oscillation Index (MOI), which affect moisture transport and rainfall distribution in this region (Luppichini et al., 2025).

5. Conclusion

This study analyses a decade (2013–2023) of high-resolution rainfall data from the Thies Clima disdrometer located in Rome (Italy), focusing on rain intermittency and its seasonal and diurnal variations. Using one of the longest available disdrometer datasets, it offers key insights to understand the characteristics of the precipitation and to assist ecohydrological management (Adirosi et al., 2024).

Seasonal analysis reveals distinct patterns: winter experiences prolonged low-intensity rain with frequent short interruptions, while summer rainfall is characterized by intense, short-duration events with fewer but longer interruptions. Autumn sees the highest total rainfall, driven by medium-sized drops and extended rain durations. A recent study similarly observed that winter rainfall tends to exhibit lower intensity with frequent but shorter interruptions (Dunkerley, 2021), aligning with our findings.

Time Averaged Rainfall Intermittency (TARI) assesses rainfall intermittency over fixed durations, showing peak values in summer, indicating higher intensity and flash flood potential (Tu et al., 2023). The recent work by Tu et al. (2023) also highlighted that high TARI values in summer indicate increased rainfall erosivity; consistently with the observed flash flood risks in our study. Intra-Event Rainfall Intermittency (IERI) examines intra-event interruptions using Minimum Inter-Event Time (MIT), with shorter MITs revealing higher intermittency in summer.

A detailed diurnal analysis shows that rainfall intermittency varies significantly throughout the day, with the highest diurnal rainfall intermittency observed around noon. In summer, rainfall intermittency peaks before noon, with a sharp decline afterward, while winter shows more consistent intermittency throughout the day. Interestingly, despite the farther apart geographical location, these diurnal patterns align with (Tu et al., 2023), who reported similar fluctuations in diurnal rainfall intensity in southern China during 2016–2021. Stratiform rain dominated autumn and winter, whereas convective rain prevailed in summer.

Understanding rainfall intermittency and its seasonal and diurnal patterns aids in predicting flooding, soil erosion, and water resource management. Future research should further explore the correlation between drop size distribution and rainfall intensity across varying climates and in light of increasing extreme rain events, and water crises in a changing climate.

CRediT authorship contribution statement

Ravi Shankar Pandey: Writing – review & editing, Writing – original draft, Visualization, Validation, Supervision, Software, Resources, Project administration, Methodology, Investigation, Funding acquisition, Formal analysis, Data curation, Conceptualization. **Alberto Carrassi:** Writing – review & editing, Visualization, Validation, Supervision, Software, Resources, Project administration, Methodology, Investigation, Funding acquisition, Formal analysis, Data curation, Conceptualization. **Federico Porcù:** Writing – review & editing, Visualization, Validation, Supervision, Software, Resources, Project administration, Methodology, Investigation, Funding acquisition, Formal analysis, Data curation, Conceptualization. **Elisa Adirosi:** Writing – review & editing, Visualization, Validation, Supervision, Software, Resources, Project administration, Methodology, Investigation, Funding acquisition, Formal analysis, Data curation, Conceptualization.

Declaration of competing interest

The authors declare that they have no known competing financial interests or personal relationships that could have appeared to influence the work reported in this paper.

Acknowledgments

This work was funded by the European Union – Next Generation EU, Mission 4 Component 2 - CUP J53D23002810006, Project DECIPHER.

Data availability

The rainfall datasets of TCD at Rome used and/or analyzed during the current study are available at https://doi.org/10.5281/zenodo.7708563 (Adirosi et al., 2023b) (version 02), and https://doi.org/10.5281/zenodo.11102745 (Adirosi et al., 2024) (version 03). Other data used are available from the corresponding author on reasonable request.

References

Adirosi, E., Porcù, F., Montopoli, M., Baldini, L., Bracci, A., Angeloni, S., Capozzi, V., Annella, C., Budillon, G., Bucchignani, E., Zollo, A.L., Cazzuli, O., Camisani, G., Minardi, G.P., Bechini, R., Cremonini, R., Antonini, A., Ortolani, A., Melani, S., Di Fabio, S., 2024. Database of the Italian disdrometer network (V03) (version V03). http://dx.doi.org/10.5281/zenodo.11102745.

Adirosi, E., Porcù, F., Montopoli, M., Baldini, L., Bracci, A., Capozzi, V., Annella, C., Budillon, G., Bucchignani, E., Zollo, A.L., Cazzuli, O., Camisani, G., Bechini, R., Cremonini, R., Antonini, A., Ortolani, A., Melani, S., Valisa, P., Scapin, S., 2023a. Database of the Italian disdrometer network. Earth Syst. Sci. Data 15, 2417–2429. http://dx.doi.org/10.5194/essd-15-2417-2023, URL https://essd.copernicus.org/articles/15/2417/2023/.

Adirosi, E., Porcù, F., Montopoli, M., Baldini, L., Bracci, A., Capozzi, V., Annella, C., Budillon, G., Bucchignani, E., Zollo, A.L., Cazzuli, O., Camisani, G., Bechini, R., Cremonini, R., Antonini, A., Ortolani, A., Melani, S., Valisa, P., Scapin, S., 2023b. Database of the Italian disdrometer network (v02). Earth Syst. Sci. Data http://dx.doi.org/10.5281/zenodo.7708563.

Angeloni, S., Adirosi, E., Bracci, A., Montopoli, M., Baldini, L., 2024. Performance of the thies clima 3D stereo disdrometer: Evaluation during rain and snow events. Sensors (Basel) 24 (5), 1562. http://dx.doi.org/10.3390/s24051562.

Atlas, D., Srivastava, R.C., Sekhon, R.S., 1973. Doppler radar characteristics of precipitation at vertical incidence. Rev. Geophys. 11, 1–35.

Bringi, V.N., Chandrasekar, V., Balakrishnan, N., Zrnić, D.S., 2003. Raindrop size distribution in different climatic regimes from disdrometer and dual-polarized radar analysis. J. Atmos. Sci. 60 (2), 354–365. http://dx.doi.org/10.1175/1520-0469(2003)060<0354:RSDIDC>2.0.CO;2, URL https://journals.ametsoc.org/view/journals/atsc/60/2/1520-0469_2003_060_0354_rsdidc_2.0.co_2.xml.

Capozzi, V., Annella, C., Montopoli, M., Adirosi, E., Fusco, G., Budillon, G., 2021. Influence of wind-induced effects on laser disdrometer measurements: Analysis and compensation strategies. Remote. Sens. 13, 3028. http://dx.doi.org/10.3390/rs13153028.

Caracciolo, D., Arnone, E., Noto, L.V., 2014. Influence of spatial precipitation sampling on hydrological response at catchment scale. J. Hydrol. Eng. 19 (3), 544–553. http://dx.doi.org/10.1061/(ASCE)HE.1943-5584.0000829.

Caracciolo, C., Napoli, M., Porcù, F., Prodi, F., Dietrich, S., C. Zanchi, e.a., 2012. Rain drop size distribution and soil erosion. J. Irrig. Drain. Eng. 138 (5), 461–469. http://dx.doi.org/10.1061/(ASCE)IR.1943-4774.0000412.

Caracciolo, C., Prodi, F., Battaglia, A., Porcù, F., 2006. Analysis of the moments and parameters of a gamma DSD to infer precipitation properties: A convective stratiform discrimination algorithm. Atmos. Res. 80 (2–3), 165–186. http://dx.doi.org/10.1016/j.atmosres.2005.07.003.

Chatterjee, C., Porcù, F., Das, S., Bracci, A., 2022. An investigation on super- and sub-terminal drops in two different rain categories and climate regimes. Remote. Sens. 14, 2515. http://dx.doi.org/10.3390/rs14112515.

Chen, B., Yang, J., Pu, J., 2013. Statistical characteristics of raindrop size distribution in the meiyu season observed in eastern China. J. Meteorol. Soc. Jpn. 91, 215–227.

Deitch, M., Sapundjieff, M., Feirer, S., 2017. Characterizing precipitation variability and trends in the world's mediterranean-climate areas. Water 9 (4), 259. http://dx.doi.org/10.3390/w9040259.

Dunkerley, D., 2012. Effects of rainfall intensity fluctuations on infiltration and runoff: rainfall simulation on dryland soils, fowlers gap, Australia. Hydrol. Process. 26 (15), 2211–2224.

Dunkerley, D., 2015. An approach to analysing plot scale infiltration and runoff responses to rainfall of fluctuating intensity. Hydrol. Process. 29 (4), 512–523. http://dx.doi.org/10.1002/hyp.10990.

Dunkerley, D., 2021. Intermittency of rainfall at sub-daily timescales: New quantitative indices based on the number, duration, and sequencing of interruptions to rainfall. Atmos. Res. 253, 105475. http://dx.doi.org/10.1016/j.atmosres.2021.105475.

Fehlmann, M., Rohrer, M., von Lerber, A., Stoffel, M., 2020. Automated precipitation monitoring with the thies disdrometer: Biases and ways for improvement. Atmos. Meas. Tech. 13, 4683–4698. http://dx.doi.org/10.5194/amt-13-4683-2020.

Friedrich, K., Higgins, S., Masters, F.J., Lopez, C.R., 2013a. Articulating and stationary PARSIVEL disdrometer measurements in conditions with strong winds and heavy rainfall. J. Atmos. Ocean. Technol. 30, 2063–2080.

Friedrich, K., Kalina, E.A., Masters, F.J., Lopez, C.R., 2013b. Drop-size distributions in thunderstorms measured by optical disdrometers during VORTEX2. Mon. Weather Rev. 141, 1182–1203. http://dx.doi.org/10.1175/MWR-D-12-00116.1.

Ganai, M., Krishna, R.P.M., Mukhopadhyay, P., Mahakur, M., 2016. The impact of revised simplified arakawa–schubert scheme on the simulation of mean and diurnal variability associated with active and break phases of Indian summer monsoon. J. Geophys. Res.: Atmos. 121 (16), 9301–9323. http://dx.doi.org/10.1002/2016JD025393.

Gunn, R., Kinzer, G.D., 1949. The terminal velocity of fall for water droplets in stagnant air. J. Meteorol. 6, 243–248.

Guo, J.C., Urbonas, B.R., 2002. Runoff capture and delivery curves for storm-water quality control design. J. Water Resour. Plan. Manag. 128 (3), 208–215.

Han, J., Braun, S.A., 2021. Microphysical characteristics of precipitation in extratropical cyclones based on GPM observations. J. Atmos. Sci. 78, 123–141.

Hassan, B.T., Yassine, M., Amin, D., 2022. Comparison of urbanization, climate change, and drainage design impacts on urban flashfloods in an arid region: Case study, new Cairo, Egypt. Water 14, 2430. http://dx.doi.org/10.3390/w14152430.

Hauser, D., Amayenc, P., Nutten, B., Waldteufel, P., 1984. A new optical instrument for simultaneous measurement of raindrop diameter and fall speed distributions. J. Atmos. Ocean. Technol. 1, 256–269. http://dx.doi.org/10.1175/1520-0426(1984)001<0256:ANOIFS>2.0.CO;2.

Huff, F.A., 1967. Time distribution of rainfall in heavy storms. Water Resour. Res. 3 (4), 1007–1019. http://dx.doi.org/10.1029/WR003I004P01007.

International Organization for Standardization, 1975. Standard atmosphere. ISO 2533:1975. https://www.iso.org/standard/7472.html.

Jaffrain, J., Berne, A., 2011. Experimental quantification of the sampling uncertainty associated with measurements from PARSIVEL disdrometers. J. Hydrometeorol. 12, 352–370. http://dx.doi.org/10.1175/2010JHM1244.1.

Janapati, J., Seela, B.K., Lin, P.-L., Wang, P.K., Tseng, C.-H., Reddy, K.K., Hashiguchi, H., Feng, L., Das, S.K., Unnikrishnan, C.K., 2020. Raindrop size distribution characteristics of Indian and Pacific ocean tropical cyclones observed at India and Taiwan sites. J. Meteorol. Soc. Jpn. Ser. II 98 (2), 299–317. http://dx.doi.org/10.2151/jmsj.2020-015, URL https://www.jstage.jst.go.jp/article/jmsj/98/2/98_2020-015/_article.

Luppichini, M., Natali, S., Columbu, A., Zanchetta, G., Bini, M., 2025. Mediterranean precipitation variability is driven by complex atmospheric mechanisms beyond the north atlantic oscillation. Nat. Commun. Earth Environ. 6, http://dx.doi.org/10.1038/s43247-025-03104-4.

Meng, W., Wang, Y., 2016. A diagnostic study on heavy rainfall induced by typhoon utor (2013) in south China: 1. Rainfall asymmetry at landfall. J. Geophys. Res.: Atmos. 121, 12781–12802. http://dx.doi.org/10.1002/2015JD024646, URL https://agupubs.onlinelibrary.wiley.com/doi/10.1002/2015JD024646.

Pandey, R.S., 2022. Statistical analysis of environmental parameters on the occurrences of tropical cyclones and earthquakes: An example from West North Pacific Region. Mar. Geophys. Res. 43 (44), 1–16. http://dx.doi.org/10.1007/s11001-022-09505-w.

Pandey, R.S., Liou, Y.-A., 2020. Decadal behaviors of tropical storm tracks in the north west pacific ocean. Atmos. Res. 246, 105143. http://dx.doi.org/10.1016/j.atmosres.2020.105143.

Pandey, R.S., Liou, Y.-A., 2022. Typhoon strength rising in the past four decades. Weather Clim. Extremes 36, 100446. http://dx.doi.org/10.1016/j.wace.2022.100446.

Pandey, R.S., Liou, Y.-A., Liu, J.-C., 2021. Season-dependent variability and influential environmental factors of super-typhoons in the Northwest Pacific basin during 2013–2017. Weath. Clim. Extremes 31, 100307. http://dx.doi.org/10.1016/j.wace.2021.100307.

Peña-Angulo, D., et al., 2020. Relationship of weather types on the seasonal and spatial variability of rainfall, runoff, and sediment yield in the western mediterranean basin. Atmosphere 11 (6), 609. http://dx.doi.org/10.3390/atmos11060609.

Peters, O., Deluca, A., Corral, A., Neelin, J.D., Holloway, C.E., 2010. Universality of rain event size distributions. J. Stat. Mech. Theory Exp. 2010 (11), P11030. http://dx.doi.org/10.1088/1742-5468/2010/11/P11030, URL https://iopscience.iop.org/article/10.1088/1742-5468/2010/11/P11030.

Porcù, F., D'Adderio, L.P., Prodi, F., Caracciolo, C., 2014. Rain drop size distribution over the tibetan plateau. Atmos. Res. 150, 21–30. http://dx.doi.org/10.1016/j.atmosres.2014.07.005.

Seela, B.K., Janapati, J., Lin, P.-L., Reddy, K.K., Shirooka, R., Wang, P.K., 2017. A comparison study of summer season raindrop size distribution between palau and Taiwan, two islands in western Pacific. J. Geophys. Res.: Atmos. 122 (21), 11,787–11,805. http://dx.doi.org/10.1002/2017JD026816, URL https://agupubs.onlinelibrary.wiley.com/doi/pdf/10.1002/2017JD026816.

Serrano-Notivoli, R., et al., 2022. Rainfall–runoff relationships at event scale in western mediterranean ephemeral streams. Hydrol. Earth Syst. Sci. 26 (5), 1243–1260. http://dx.doi.org/10.5194/hess-26-1243-2022.

Seto, S., Iguchi, T., Oki, T., 2013. The basic performance of a precipitation retrieval algorithm for the global precipitation measurement mission's single/dual-frequency radar measurements. IEEE Trans. Geosci. Remote Sens. 51, 5239–5251. http://dx.doi.org/10.1109/TGRS.2012.2231686.

Sharma, S., Konwar, M., Sarma, D.K., Kalapureddy, M.C.R., Jain, A.R., 2009. Characteristics of rain integral parameters during tropical convective, transition and stratiform rain at gadanki and its application in rain retrieval. J. Appl. Meteorol. Clim. 48, 1245–1266. http://dx.doi.org/10.1175/2008JAMC2035.1.

Thurai, M., Bringi, V.N., 2005. Drop axis ratios from a 2D video disdrometer. J. Atmos. Ocean. Technol. 22, 966–978. http://dx.doi.org/10.1175/JTECH1767.1.

Tokay, A., Bashor, P.G., Wolff, K.R., 2008. Raindrop size distribution measurements in tropical cyclones. Mon. Weather Rev. 136 (5), 1669–1685. http://dx.doi.org/10.1175/2007MWR2122.1.

Tokay, A., D'Adderio, L.P., Porcù, F., Wolff, D.B., Petersen, W.A., 2017. A field study of footprint-scale variability of raindrop size distribution. J. Hydrometeor. 18, 3165–3179. http://dx.doi.org/10.1175/JHM-D-17-0003.1.

Tokay, A., Kruger, A., Krajewski, W., 2001. Comparison of drop-size distribution measurements by impact and optical disdrometers. J. Appl. Meteorol. 40, 2083–2097. http://dx.doi.org/10.1175/1520-0450(2001)040<2083:CODSDM>2.0.CO;2.

Tramblay, Y., et al., 2023. Changes in mediterranean flood processes and seasonality. Hydrol. Earth Syst. Sci. 27 (15), 2973–2987. http://dx.doi.org/10.5194/hess-27-2973-2023.

Treppiedi, D., Cipolla, G., Noto, L., 2022. Convective precipitation over a mediterranean area: From identification to trend analysis starting from high-resolution rain gauges data. Int. J. Climatol. 43 (1), 293–313. http://dx.doi.org/10.1002/joc.7758.

Tu, A., Zeng, J., Liu, Z., Zheng, H., Xie, S., 2023. Effect of minimum inter-event time for rainfall event separation on rainfall properties and rainfall erosivity in a humid area of southern China. Geoderma 431, 116–123. http://dx.doi.org/10.1016/j.geoderma.2023.116332.

Ulbrich, U., Atlas, H., 2007. The structure of precipitation in convective and stratiform rainfall. Atmos. Res. 85 (4), 339–349.

UN-Water, 2019. Policy Brief: Climate Change and Water. Tech. rep., UN-Water Expert Group on Water and Climate Change, URL https://www.unwater.org/app/uploads/2019/07/UN-Water_Water-and-Climate-Policy-Brief_unedited-1.pdf.

Weatherspark.com, 2025. Average weather in rome, Italy year-round. URL https://weatherspark.com/y/71779/Average-Weather-in-Rome-Italy-Year-Round.

Williams, C.R., et al., 2014. Describing the shape of raindrop size distributions using uncorrelated raindrop mass spectrum parameters. J. Appl. Meteor. Clim. 53, 1282–1296. http://dx.doi.org/10.1175/JAMC-D-13-076.1.

Wood, N.B., L'Ecuyer, T.S., Vane, D.G., Stephens, G.L., Partain, P., 2013. Level 2C snow profile process description and interface control document. Tech. rep., JPL, p. 21, URL https://www.cloudsat.cira.colostate.edu/cloudsat-static/info/dl/2c-snow-profile/2C-SNOW-PROFILE_PDICD.P1_R05.rev0_.pdf.

Yuter, S.E., Kingsmill, D.E., Nance, L.B., Löffler-Mang, M., 2006. Observations of precipitation size and fall speed characteristics within coexisting rain and wet snow. J. Appl. Meteor. Clim. 45, 1450–1464.

Zeng, Y., Yang, L., Zhou, Y., Tong, Z., Jiang, Y., 2022. Statistical characteristics of summer season raindrop size distribution in the western and central tianshan mountains in China. J. Meteorol. Soc. Jpn. Ser II 100, 855–872. http://dx.doi.org/10.2151/jmsj.2022-044.

Zhao, Y., Xia, J., Xu, Z., Qiao, Y., Shen, J., Ye, C., 2023. Impact of urbanization on regional rainfall-runoff processes: Case study in jinan city, China. Remote. Sens. 15, 2383. http://dx.doi.org/10.3390/rs15092383.